On the interactions between carbohydrates and immune cells

Steuten, K.

Chapter 2

An automated processing pipeline for Glyco-PAINT

Kas Steuten[1], Johannes J.A. Bakker[1], Ward Doelman[1], Diana Torres-García[1], Christian Kurts[3], Roger Riera[2], Lorenzo Albertazzi[2] & Sander I. van Kasteren[1]

[1] Department of Chemical Biology and Immunology, Leiden Institute of Chemistry, Leiden, The Netherlands
[2] Department of Biomedical Engineering and Institute for Complex Molecular Systems, Eindhoven University of Technology, Eindhoven, the Netherlands
[3] Institute of Experimental Immunology, University of Bonn, Bonn, Germany

Parts of this chapter are published as: Steuten, K. *et al.*, *Nature Communications*, 17, 886 (**2026**).

2.1 Introduction

The recently reported Glyco-PAINT technique enables measurement of glycan binding kinetics on live cells.[1] This method enables the quantification of glycan off-rates, relative on-rates and receptor movement on the surface of living cells. Glyco-PAINT exploits the transient interaction between fluorescently-labeled sugars and their receptors to generate single molecule binding events, analogous to those induced by the semi-complementary DNA-strands in conventional Point Accumulation for Imaging in Nanoscale Topography (DNA-PAINT)-imaging.[2] Accumulation of these binding events over time allows for the mapping of receptor-ligand interactions on the cell surface and subsequent derivation of kinetic parameters such as on-rate, off-rate and diffusion coefficients on a per-cell basis derived from single-molecule binding information.

In the initial report, the Glyco-PAINT method was demonstrated on a Mannose Receptor (MR) overexpression CHO cell line. This system proved itself very useful for developing the technique due to its homogeneous receptor expression. It fails, however, to capture the biological complexity of lectin expression on primary cells. For example, myeloid immune cells such as dendritic cells and macrophages, express a diverse array of CLRs for sensing aberrant glycosylation and thus display a far more complex lectin expression profile. This complexity emerges from a variety of factors: binding of the receptors to ligands is weak and often multivalent, multiple receptors have overlapping specificities, and the surface expression patterns of CLRs can be highly dynamic. These lectins can exist as monomers, multimers, and even form heterodimeric complexes.[3,4] Various factors, such as the activation state of the immune cell, can modulate the expression levels of these lectins, and alter the sub-cellular distribution between the surface and intracellular storage pools.[5,6] The resulting dynamic and heterogeneous surface expression leads to significant variability in receptor-ligand interactions.

To complicate matters further, myeloid cells also present a repertoire of glycans that can serve as ligands for their own lectins. These can modulate signaling pathways through ligand competition and receptor clustering. Polarization of immune cells also affects the expression of these *cis*-ligands, adding yet another layer of complexity to carbohydrate-immune lectin biology.[7] The final complicating factor in CLR-binding and signalling is that the affinities of C-type lectin domains (CTLs) for their ligands are weak (K_D in the µM to mM range).[8] This complicates the detection and precise study of these interactions. Together with the intrinsic chemical complexity of glycan ligands, these factors have made it exceedingly difficult to establish clear relationships between glycan binding properties and lectin function, particularly as studying these lectins out of their native context removes many of these modulating factors.

We envisaged that Glyco-PAINT could be a powerful technique to unravel the complexity of lectin binding on primary myeloid cells, as the single-molecule as well

as the live-cell aspects of the technique are ideal for studying these capricious receptors within their native environment on the myeloid cell surface. This chapter describes the methodological changes to the original Glyco-PAINT method that were needed to obtain quantitative binding information from mannose glycan binding to the MR on myeloid cells. The analysis algorithm is able to independently process large volumes of Glyco-PAINT recordings in such a way that binding event concentration, off-rates, diffusion coefficients and displacement can be determined for the highly heterogeneous and disperse binding observed across the cell basal membrane of DCs and macrophages.

2.2 Results

2.2.1 Quantifying glycan-lectin binding on dendritic cells

Our first aim was to determine whether the Glyco-PAINT methodology could be used to study binding events on the surface of primary bone-marrow derived mouse dendritic cells (BMDCs).[9] Unlike the overexpression system used previously, BMDCs are characterized by heterogeneous and dynamic receptor expression of multiple lectins, multiple of which are capable of binding mannosylated ligands, and structural features such as tight focal adhesions and podosomes, that may exclude binding events from the TIRF plane.[10,11] Initially, the quantification of binding to BMDCs was attempted using a small library of labeled mannose glycans consisting of glycoclusters **8**, **10**, **11** and **13** (**Figure 2.1**).

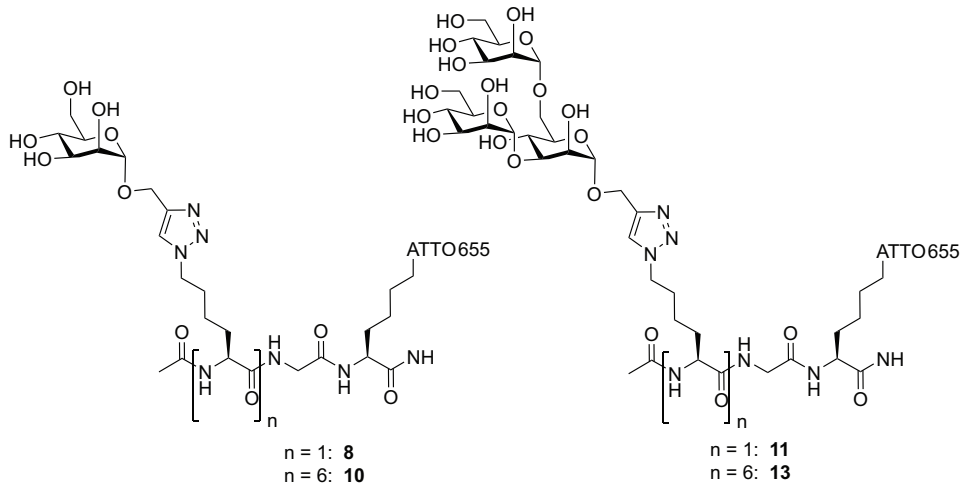

Figure 2.1: Mono- and trimannoside glycoclusters from Riera *et al.*[1] that were used in this chapter.

Here, binding events of the different clusters to the DCs could clearly be seen in the Glyco-PAINT recordings (**Figure 2.2**), but no significant differences were observed between the probes for neither relative on-rate, nor in the average ligand dwell time τ (or k_{off}^{-1}) which is determined via fitting a one-phase exponential decay function through distribution of binding lengths per ROI as in Riera *et al.*[1] (**Figure 2.2e, f**). When comparing this analysis to control experiments in CHO-MR cells, binding patterns in coherence with the original report were observed (**Figure S2.1**). Interestingly, the track reconstructions of glycans binding to BMDCs showed a very high variance in the density of binding events between individual cells—with some cells devoid of binding events, and others showing large numbers of events—and even between different regions of the basal membrane of a single cell (**Figure 2.3b**). Areas rich in binding events were observed overlapping with brightfield-defined cell outlines (**Figure 2.3b**, green areas). However, large areas of the cell basal membrane were also devoid of any binding event density (**Figure 2.3b**, red areas and **Figure 2.2a-d**) and some areas outside the brightfield-defined cell surface appeared to be also engaging in binding events (**Figure 2.3b**, blue areas), suggesting the presence of receptors on the ultrathin dendrites. In contrast, this heterogeneity was not observed for CHO-MR cells (**Figure 2.3a**, green areas and **Figure S2.1**).

The fundamental assumption that underpins the Glyco-PAINT method is that the second-order rate of the binding reaction (r) depends on the rate constant k_{on}, the density of receptors on the cell [R] and the probe concentration [L]:

$$r = k_{\text{on}}[R][L]$$

The observation of highly dispersed binding events on the dendritic cell surface meant that this assumption was incorrect, because [R] is no longer homogeneous over the basal membrane of every cell. This in turn implies that the per-cell relative on-rate was an irrelevant parameter for the study of primary cells. The off-rates too are averaged on a per-cell basis as they are integrated over the complete area whereas only a subsection contains binding-enabled lectins. Taken together, the observed highly heterogeneous binding event distribution calls for a different surface area definition in order to obtain meaningful quantification of kinetic parameters.

2.2.2 Glyco-PAINT-APP

The Glyco-PAINT-Automated Processing Pipeline (Glyco-PAINT-APP) was developed to address these problems associated with cellular heterogeneity. Instead of using the whole cell as the averaging unit, the basal membrane was segmented into squares to account for the subcellular variation of binding events (**Figure 2.3a-b**, right images). This allows a more precise quantification of glycan binding kinetics within localized areas whilst ignoring the areas in which no binding events occur. An additional boon to this approach was that this method allowed for the automation of the workflow,

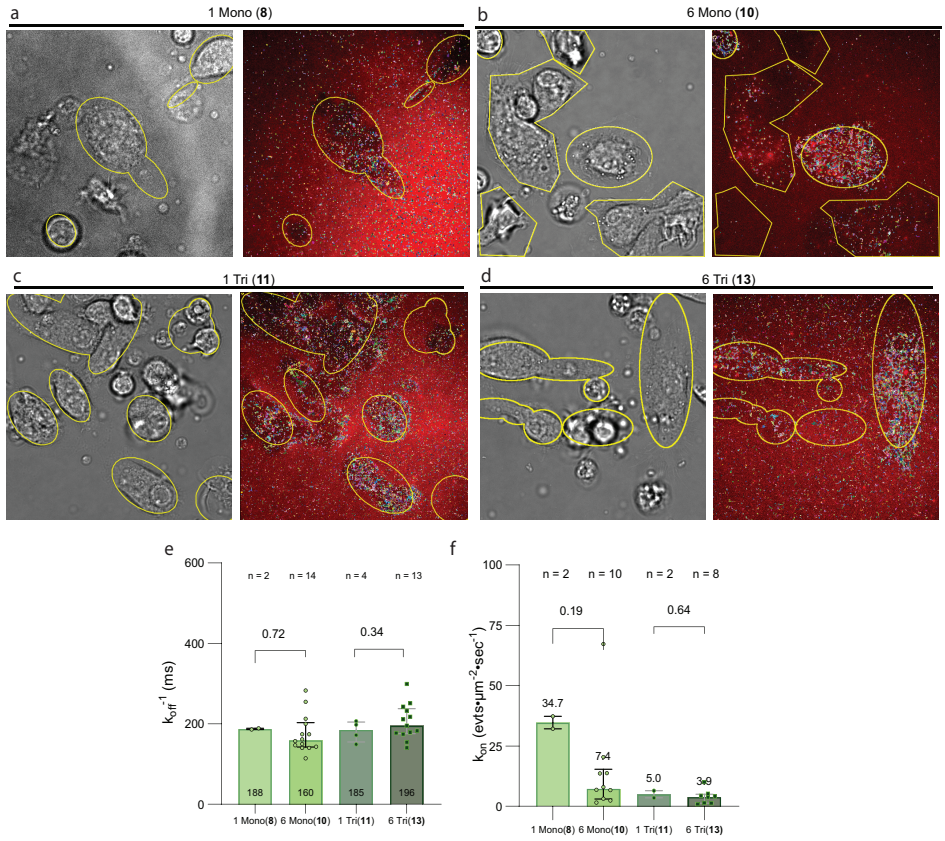

Figure 2.2: Manual analysis of glycan binding on dendritic cells is complicated by intrinsic cell heterogeneity and results in averaging artefacts. (**a**) BMDCs were incubated with 5 nM of fluorescent mannoside **8** in a live cell imaging chamber and a brightfield image was captured followed by a 2000 frame Glyco-PAINT recording. Closely-linked spots in subsequent frames were reconstructed into tracks representing binding events using the ImageJ TrackMate plugin and background filtering was performed by manual cell definition using ROI drawing (yellow outlines). (**b-d**) Identical analysis for glycans **10**, **11** and **13**, respectively. (**e**) Quantification of the number of events per area which is a relative measure of k_{on}. (**f**) The average k_{off}^{-1} for these events determined by fitting a one-phase exponential decay function over the binding event duration distribution histograms. n, depicts the number of recordings that were analyzed in total and were acquired over at least 3 biological replicates. However, not all recordings passed quality selection as detailed in methods section. Significance was assessed using two-way ANOVA followed by a Tukey post-hoc test. Tracks are colored randomly. Bar graphs and error bars represent mean ± interquartile range.

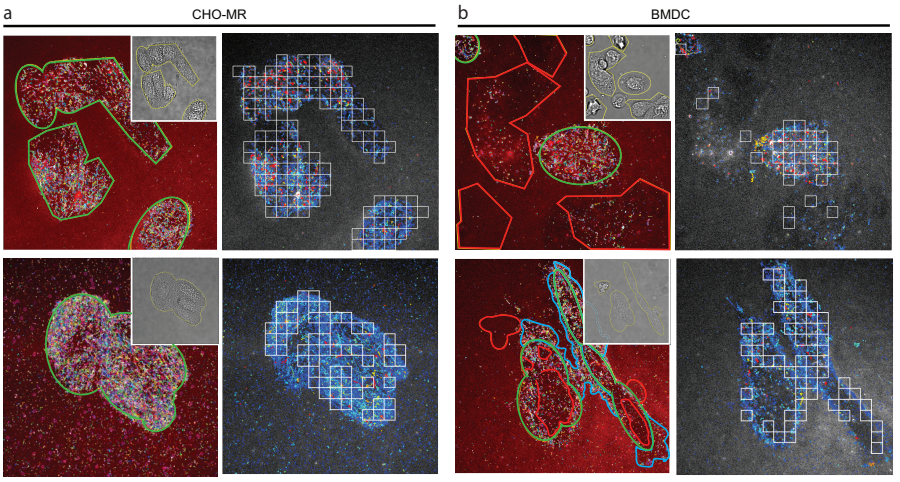

Figure 2.3: Glyco-PAINT-APP allows for subcellular analysis of immune cell lectin binding (**a**) Left images (with red background): original Glyco-PAINT analysis of fluorescent mannose glycan binding to CHO-MR cells. ROIs are drawn using brightfield-defined cell contours (inset, yellow outlines) and areas where binding events are overlapping with cell areas are outlined in green. Binding trajectories are randomly colored. Right images (with gray background): Grid-based identification of binding events using Glyco-PAINT-APP. Automatically defined white squares show an independent selection of cell-related binding events and define the area over which events are integrated. (**b**) Same as **a** but for BMDC. In the left images, manual outlining of non-overlapping areas devoid of binding events arising from primary cell intrinsic heterogeneity in red and areas engaging in binding events but outside of brightfield-defined cell outlines in blue.

compared to the previous requirement for a manual identification of the cell outlines, thereby accelerating analysis speed. The Glyco-PAINT-APP is schematically outlined in **Figure 2.4** (and described in full detail in the Supplementary Manual).

Glyco-PAINT-APP starts by subjecting sets of microscope recordings of Glyco-PAINT experiments to single particle tracking analysis using TrackMate.[12] This yields output files containing spatial information pertaining to each spot in each frame of the Glyco-PAINT recording. Tracks, consisting of closely linked spots through multiple consecutive frames, can then be generated and their duration, and movement-based parameters (such as distance traveled, start-point, end-point, and displacement) determined. The Glyco-PAINT-APP then processes the recordings by segmenting the field of view in a raster of squares (typically 20x20 squares per field of view), rather than manually outlining cells. The kinetic information is then quantified for each of these squares, rather than per cell. This allows for selection of only those regions of the cell surface on which binding events take place. This selection is done based on the number of events that occur and that meet a given set of quality control parameters. The quality control parameters are taken from the TrackMate-output, and in addition, we have included the following new quality control parameters:

- Density Ratio: the ratio of events in a square divided by the number of events in the lowest binding 10% of squares that contain at least one event.
- Maximum Variability: a score for event homogeneity within a single square.
- Connectivity: a measure for how isolated a square can be within the image.
- R Squared: the quality (R^2) of the one-phase exponential decay fit.
- Minimum number of Tracks To Calculate Tau: threshold for including data in off-rate calculations.

The interactive tuning of these parameters is done using the "Select Squares" window and the effects on the recording can be assessed by direct visual feedback from the "Recording Viewer" (**Figure 2.4**) where the tracking overlay with grids and bright-field image are displayed side-by-side. This allows for user-informed data curation. Once the squares are selected, kinetic parameters including glycan on- and off-rates, diffusion coefficients, speed, displacement and maximum, average, or total binding event duration can be displayed for each square per recording using the heatmap toggle function in the "Recording Viewer" (**Figure 2.4**). The "Compile Project" built-in modality can integrate kinetic data from multiple experiments obtained from biological replicates within a single project and can generate a merged output file to which statistical analysis can be applied with scientific graphing software of choice (R Studio, GraphPad Prism, etc.). In **Table 2.1** an overview of all kinetic and statistical output parameters is presented together with a description.

With this automated analysis pipeline in place, the approach was first validated using the binding of glycoclusters **8**, **10**, **11** and **13** to DCs. These ligands cover a range of affinities from the initial Glyco-PAINT report and helped determine how variation of each parameter affected τ, track mobility, the relative on-rate and density ratio. This sweep included varying spot detection threshold, track reconstruction parameters, and grid size. The parameter sensitivity analysis for tracking and spot detection parameters is depicted with heatmaps of each scenario in (**Figure S2.2a-b**). From this analysis, we first determined how varying the parameters affected the number of squares that passed selection criteria per image for CHO-MR versus the MR-negative CHO-WT (**Figure 2.5a**). We found that any of the parameter values for Gap Closing Max Distance, Max Frame Gap and Linking Max Distance were able to select squares engaging in MR-mediated binding events from CHO-WT background. For the Minimum Nr Of Spots, we found that tracks should consist of a minimum of 3 spots, since the number of selected squares when allowing minimum track lengths of 2 spots in CHO-WT, were inflated close to CHO-MR levels. This implies that binding events spanning only 2 frames (100 ms), can be considered MR-unrelated background whereas a minimum of 4 spots appeared to result in overly stringent filtering (**Figure 2.5a**). For the Threshold, we found that values > 4 were resulting in accurate separation between CHO and

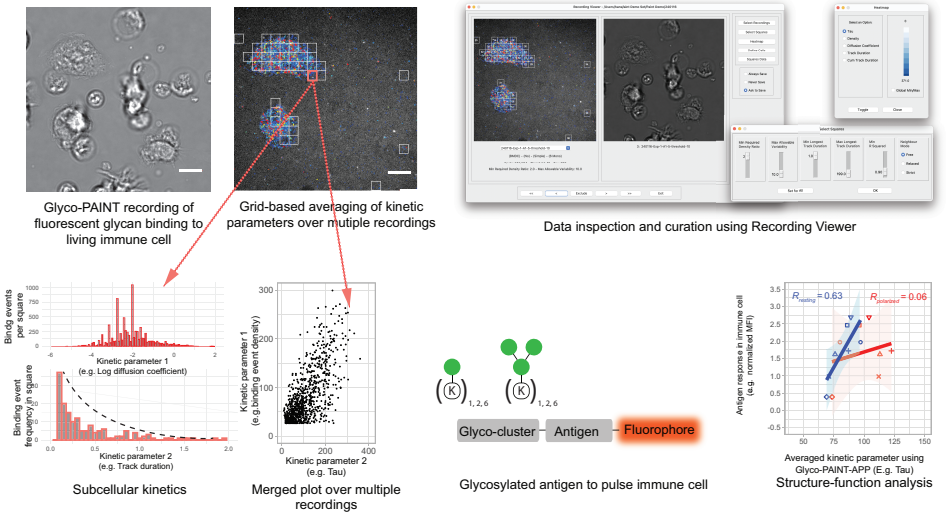

Figure 2.4: Overview of the Glyco-PAINT-APP workflow. Primary immune cells are cultured in a live-cell imaging chamber and a brightfield image is recorded. After addition of a fluorescent probe, spots are recorded using PAINT imaging and reconstructed into tracks reflecting glycan binding events which are then subdivided into squares of variable size depicting subcellular regions of live immune cells. Kinetic parameters such as on-, off-rates and diffusion coefficients of glycan ligands averaged per individual square can then be interpreted, analysed and filtered using the Recording Viewer tool and displayed as heatmaps, histograms or scatterplots. Kinetic parameters derived using the algorithm can subsequently be correlated to functional effects of resting or polarized immune cells. Scalebars represent 10 µm, data figures indicate representative illustrative data.

CHO-MR. Next, we further analysed the sensitivity of track and spot detection parameters on the kinetic parameters off-rate, on-rate and diffusion coefficient. Here, it was found that of the tracking parameters, Min Nr Of Spots had a large influence on the average τ since short duration tracks are discarded. In contrast, median off-rates were largely independent of threshold settings above 3 (**Figure 2.5b**), median number of detected events (on-rate) remained constant above 5 (**Figure 2.5c**) and also diffusion coefficients did not vary above 4 (**Figure 2.5d**). However, the density ratio appeared to remain constant above a threshold of 8 (**Figure 2.5e**). To summarize, the track reconstruction parameters as indicated in methods were kept constant for all analysis and the spot detection threshold was initially set at 5 since for this value the detection bias was minimized. If > 1,500,000 spots per recording were detected, the threshold was increased to a maximum of 20 in steps of 5 due to computational limitations.

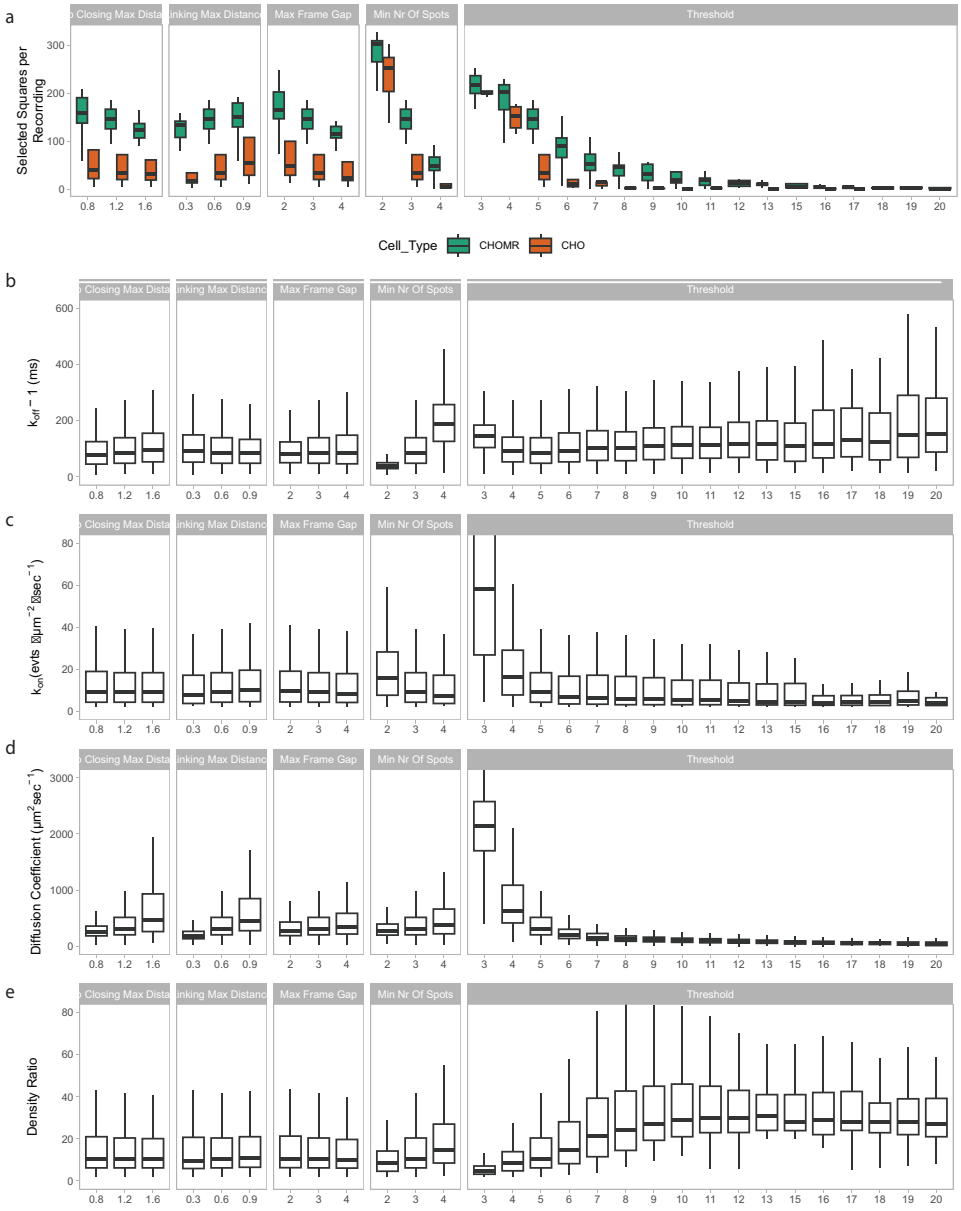

Figure 2.5: Parameter sweep of TrackMate spot detection and track reconstruction settings (**a**) For each parameter setting as in **Figure S2.2** the resulting number of squares that passed selection in a 20×20 grid, and filtered with Density_Ratio > 2, R_Squared ≥ 0.9, and Nr_Tracks/Square > 200 is shown as boxplots comparing pooled data for glycans **8**, **10**, **11** and **13** binding to CHO versus CHO-MR. (**b-e**) Same as in **a** for Glyco-PAINT-APP kinetic parameters derived from CHO-MR binding only. Boxplots show median (line) and interquartile range (box); whiskers extend to ±1.5×IQR. Outliers beyond whiskers are omitted.

2.2.3 Subcellular analysis of immune cell lectin binding

We next applied Glyco-PAINT-APP with these settings to the profiling of glycan binding events on DCs. For these intrinsically heterogeneous cells, we optimized the grid size to avoid averaging artefacts. For this we used the complete dataset of mannose ligands binding to BMDC, which consists of approximately 400 different recordings (each of standard 81 x 81 µm², 512 x 512 pixels, and 2000 frames at 20 frames per second). Our analysis demonstrated that 20 squares per axis provided an optimal balance between statistical robustness of the off-rate fit (R^2 >0.9), the number of binding events per square, and the minimization of averaging artifacts (**Figure 2.6**). Off-rates (τ) did not vary with square size (**Figure 2.6b**), but on-rates and the density ratio diverged with square size (**Figure 2.6c-d**). With this analysis pipeline in hand, we set out

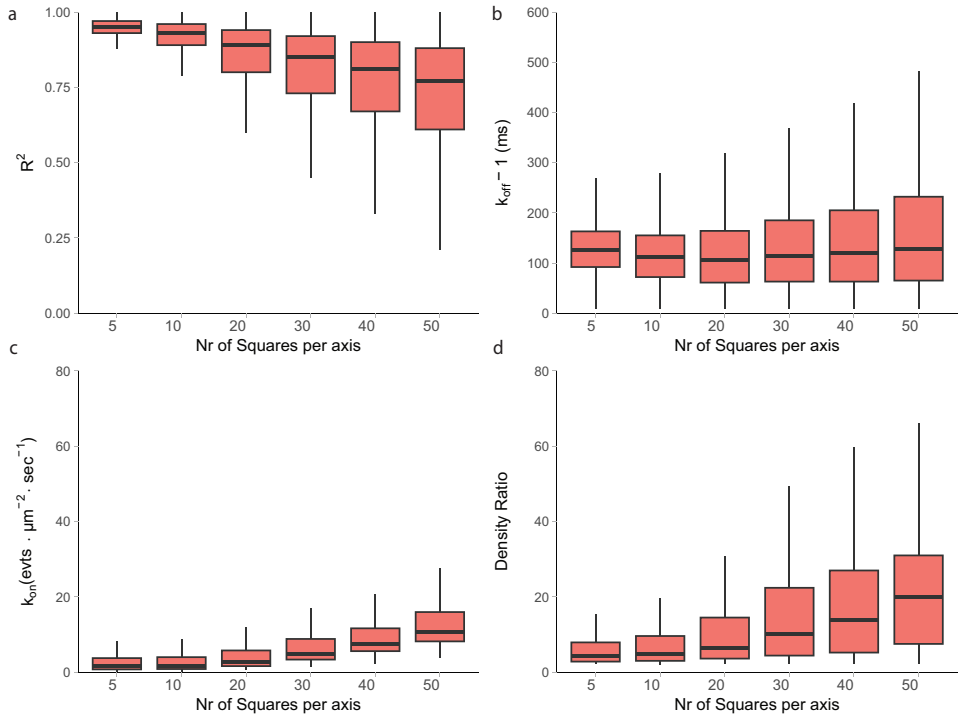

Figure 2.6: Quantification of the effects of grid size on Glyco-PAINT-APP parameters Analysis of the effect of different grid sizes on statistical (**a**) and kinetic (**b-d**) parameters for all glycans binding to BMDC. Boxplots show median (line) and interquartile range (box); whiskers extend to ±1.5×IQR. Outliers beyond whiskers are omitted.

to reprocess the recordings of the mannose probe library on primary DCs for which the original Glyco-PAINT procedure had not yielded any significant differences in binding between the different glycoforms. The square-based analysis for DCs is dis-

played in **Figure 2.7** (for the same recordings as in **Figure 2.2** and extended in **Figure S2.3** for the library of mono- and trimannosides). **Figure 2.7b** and **f** show that the APP-algorithm was able to independently distinguish areas with binding event density from background using filtering based on the previously optimized parameter settings. The added advantage of this approach is that binding events that fell outside

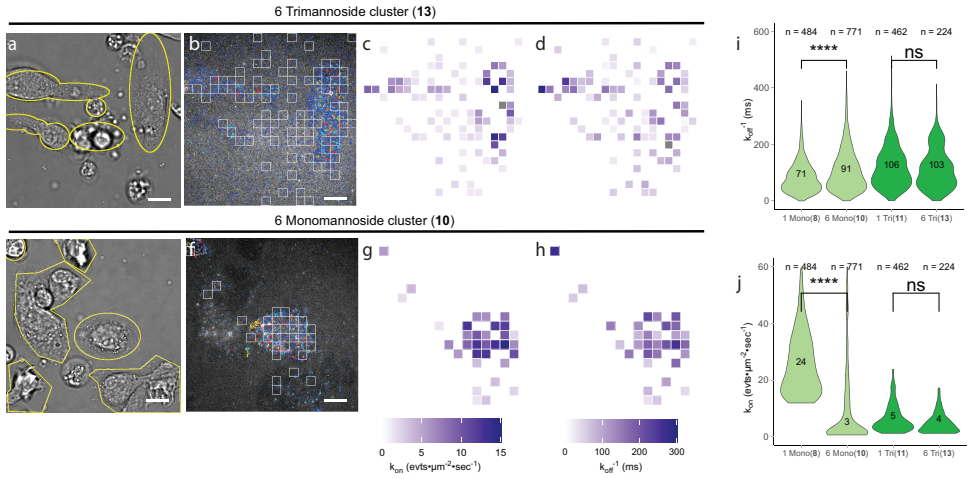

Figure 2.7: Subcellular analysis of glycan binding on dendritic cells resolves averaging artefacts (**a**) brightfield image of live BMDCs. (**b**) Reconstruction of binding events recorded with 5 nM trimannoside glycan **13** processed using a 20×20 grid with all squares that have passed selection criteria (Density_Ratio > 2, R_Squared ≥ 0.9, and Nr_Tracks/Square > 20) displayed by white outlines (**Figure S2.4a-b** show the same set of images for glycan clusters **11** and **13**). (**c**) Heatmap projection of the number of binding events/square showing the high heterogeneity of binding events even between the selected squares on the same cell. (**d**) Heatmap display of k_{off}^{-1} per square. (**e-h**) The same as **a-d** but for glycan cluster **10**. (**i-j**) Violin distribution plots and median value of k_{on} and k_{off}^{-1} for all glycans **10-13**. n, depicts the number of squares that were analyzed per violin. Significance was assessed using two-way ANOVA followed by a Tukey post-hoc test. Scalebars represent 10 µm. Tracks in **b** and **f** are colored from short to long track length (light blue to red).

brightfield-invisible features of the DC are now also included in the analysis. The thus observed binding rates in different areas of the cell basal membrane can be visualised as heatmaps in **Figure 2.7c**, **d** and **g**, **h**. The grid-based analysis by Glyco-PAINT-APP also improved the effective selection of cell areas engaged in binding events for mono- and trimannoside-based probe binding to CHO-MR (**Figure S2.4**), highlighting the omnipresence of microheterogeneity even in overexpression systems. Taken together, this method allows for precise analysis of glycan-lectin interactions on live immune cells with intrinsically heterogenic expression avoiding the emergence of averaging artefacts as in the original Glyco-PAINT analysis. Some interesting parameters began to emerge from the approach. For example, a discrepancy between areas of high num-

ber of binding events (**Figure 2.7c**, **g**) and areas with long average duration of binding (**Figure 2.7d**, **h**) within the same cell could be seen on DCs.

2.3 Discussion and conclusion

This chapter describes the single-molecule quantification of glycan-lectin binding on primary immune cells. While quantification of glycan-lectin binding using glycan arrays[13], SPR[14] or ELISA-based[15] technologies with immobilised ligands has yielded a wealth of information related to binding preferences of individual lectins to glycans and vice versa, it has never done so in the context of the living cell surface, where the glycocalyx, other lectins, and the constant movement of the membrane can affect glycan binding. Glyco-PAINT-APP offers a significant technological advance that enables the study of glycan-lectin binding in its native context. It is particularly potent, as it now allows the quantification of binding of non-homogeneous distributions of binding events on the cell surface. The method starts with PAINT recordings of glycan binding to heterogeneous, semi-adherent, cell types and can extract kinetic information in the form of off-rates, relative on-rates, diffusion coefficients, displacement and speed of the receptor-ligand interaction in an unbiased and high-throughput manner whilst respecting the subcellular variations typically associated with live cells of primary origin. We believe that the Glyco-PAINT-APP can be of use to expand the information that can be obtained from all PAINT-like technologies where the field is moving toward the use of physiological ligands such as peptides, glycans and proteins as imaging probes beyond the original DNA-PAINT method.[16–18] Furthermore, our approach could aid in fundamental investigations into the dynamics of immune cell lectins of other families such as the Siglecs. It could also be of use for structure-function or target-engagement studies of other ligands that have a typical low affinity interaction with their receptors such as low-affinity antibodies, peptides, or TCR-pMHC interactions[19,20] or other interactions where (weak) binding affinities do not appear to correlate with function, such as the recently reported anti-CD40 antibody library, where affinity reduction led to increased receptor engagement.[21] We acknowledge several limitations of the Glyco-PAINT-APP technology for primary cells that should be considered when interpreting results. First, accurate discrimination between true binding events and background noise remains challenging, making appropriate negative biological controls essential. In the case of myeloid cells, such controls are particularly difficult to obtain, as these cells rarely lack lectin-binding partners due to the high promiscuity of glycan–lectin interactions and the presence of multiple, often weak, binding partners—some of which may not yet be identified. In this context, the CHO/CHO-MR cell line pair provides an optimal single-lectin control, as wild-type CHO cells lack any CLR expression (at least from LC-MS/MS proteomics-based quantification).[22] Second, lectin trafficking from the plasma membrane to intracellu-

lar compartments introduces additional complexity. Additional factors that may bias the observed kinetics include degradation of glycan probes by glycolytic enzymes and pH-dependent effects on binding stability.

2.4 Methods

Acknowledgments Nico Meeuwenoord and Hans van Elst are acknowledged for their assistance with HPLC and SEC purifications. We thank the Animal Research Facility (ARF) for mouse breeding and colony management.

Ethical Statement All animal experiments received approval from the Dutch Central Authority for Scientific Procedures on Animals (CCD) on license number AVD1060020198832 and were conducted in accordance with the European Union Directive 2010/63/EU, recommendation 2007/526/EC.

Data and code availability The Glyco-PAINT-APP software package is available on GitHub:
`https://github.com/Leiden-chemical-immunology/Glyco-PAINT`. Installation instructions, demonstration datasets and a software manual are also available via GitHub. Representative raw recordings and all processed tracking data have been deposited in the Zenodo repository under DOI:
`https://doi.org/10.5281/zenodo.17485662`

Mice Male C57Bl/6J were purchased from Charles River. The animals were provided with water and food *ad libitum* under a 12:12 day/night cycle. Mice ranging from 8 to 15 weeks old were euthanized by cervical dislocation before harvest of lymphoid organs and/or thigh bones, femur, and tibia.

2.4.1 Cell culture

Bone marrow-derived dendritic cells (BMDC) Bone marrow (BM) was isolated from femurs, tibias, and thigh bones of WT or $MR^{-/-}$ C57Bl/6J mice via centrifugation (1900 rcf, 4.5 min) of scissor-cut bones that were placed inside a standard 200 µL micropipette tip in a 1.5 mL tube. The resulting pellet was subjected to red blood cell (RBC) lysis by resuspending in 0.5 mL of ammonium chloride-potassium (ACK) lysis buffer (Gibco, A1049201). After 3 min incubation at room temperature, the suspension was filtered over a 70 µm filter (Falcon, 352350), rinsed with 5 mL PBS and washed once with PBS by 5 min centrifugation at 300 rcf at room temperature. Thus obtained BM was resuspended at 1×10^6 cells/mL in 15 cm uncoated culture dishes (Sarstedt, 82.1184.500) in complete RPMI-1640 (Capricorn, RPMI-A) supplemented

with 10% heat-inactivated fetal calf serum (FCS, Gibco, A5670701), penicillin (100 I.U./mL) and streptomycin (50 µg/mL) (Gibco, 15140148), 2 mM GlutaMAX (Gibco, 35050061), 50 µM 2-mercaptoethanol (Gibco, 31350010) and 20 ng/mL mGM-CSF (Peprotech, 315-03) and cultured in a humidified incubator at 37 °C and 5% CO_2. On day two, 5 mL of fresh medium was added and on day four cells were reseeded in fresh medium at 1×10^6/mL. Cells were used for microscopy and T cell activation experiments on day 7 or 8.

CHO–MR cells The CHO–MR cell line was kindly provided by Luisa Martinez-Pomares[23] and cultured in DMEM/F12 without phenol red (Gibco, 21041025), supplemented with 10% FCS, penicillin (100 I.U./mL), streptomycin (50 µg/mL), and selection antibiotic G418 (0.6 mg/mL). A layer of adherent cells was washed with PBS and cells were harvested by 10 min incubation with 2 mM EDTA in PBS and subcultured approximately twice per week at a 1:5 split when cells reached 70–80% confluency.

2.4.2 Imaging and analysis

Glyco-PAINT optical setup Single-molecule imaging was performed on a Nikon Ti2 N-STORM system equipped with a TIRF module, Z piezo element, perfect focus system for axial drift correction and an OkoLab incubator with temperature and CO_2 controller (37 °C and 5% CO_2) for live-cell imaging. Recordings were acquired using the 647 nm excitation laser (160 mW, 1.9 kW/cm^2). Upon laser excitation, fluorescence was collected by a 100x 1.49 NA oil-immersion objective, passed through a quad-band dichroic mirror (97335 Nikon), and detected by a Hamamatsu ORCA Flash 4.0 CMOS camera with 160 nm pixel size. The signal was collected using the following settings: 512x512 pixel region, no binning, pixel depth 16-bit, exposure time 50 ms, live-cell observation and 2D-STORM (lens out), zoom 1x, lens x0.4, and for live-cell observation at 37 °C the correction collar was set to position 8160.

Acquisition of Glyco-PAINT recordings 5×10^4 CHO–MR, 1×10^5 BMDC or BMDM were seeded in 8-well glass-bottomed microscopy slides (Ibidi, 80827) in complete medium. After equilibration in the microscope incubator, fluorescent glycan was added at 5 nM for CHO–MR and 10 nM for BMDC or BMDM experiments. Then, cells were brought into focus using brightfield illumination and 2,000 frames (at 50 ms intervals) were recorded within a single field-of-view at 40–60% of maximum 647 nm laser power using TIRF illumination. For indicated experiments, Cytochalasin D (Focus Biomolecules) was added to a final concentration of 10 µM for 30 min prior to acquisition.

ROI-based analysis of Glyco-PAINT recordings TrackMate was run manually using the Fiji plugin.[12] The LoG spot detection algorithm was applied with an object radius of 0.5 µm, with pre-processing with median filter and sub-pixel localization unchecked. Threshold values were set to 5, 10 or 15 such that no more than 1,500,000 spots were detected and kept identical per experimental condition. Next, single-particle tracking was performed using the Simple LAP tracker algorithm with a maximum frame gap of 3, a max linking distance of 0.6 µm and a gap closing max distance of 1.2 µm. Tracks with only two spots were discarded. Manual Regions of Interest (ROIs) were drawn in individual recordings using Fiji based on brightfield-defined cell outlines. The number of tracks residing within the ROI were compared with the number of tracks outside the ROI to establish a ratio of cell/glass density. Only recordings for which that ratio exceeded 2 were considered for further analysis. For all remaining recordings, the k_{on}, k_{off}^{-1} and MSD were calculated for tracks within the ROI according to Riera *et al*.[1] Statistical analysis and plotting was performed using GraphPad Prism v10.

Glyco-PAINT-APP analysis of recordings Processing of recordings using Glyco-PAINT-APP was performed as described in a step-by-step procedure that can be found on GitHub. For the TrackMate processing, a batch file (Experiment Info.csv) containing the experiment metadata and tracking parameters was created. Threshold values were set to 5, 10 or 15 such that no more than 1,500,000 spots were detected. Recordings were then processed in TrackMate using the 'Run TrackMate Batch' plugin provided by the Glyco-PAINT-APP. Spot detection and tracking by TrackMate was performed as indicated in the batch file using the Simple LAP tracker algorithm with a maximum frame gap of 3, a max linking distance of 0.6 µm and a gap closing max distance of 1.2 µm. Tracks with only two spots were discarded. For the parameter sensitivity analysis, each tracking or spot detection was varied as indicated whilst the others were kept at the aforementioned values (basis scenario).

With the Glyco-PAINT-APP utility 'Generate Squares', a grid of squares was overlaid and kinetic properties for each square were calculated. Default parameters for grid processing are (deviations are mentioned in figure captions): Nr of Squares in row: 20, Minimum Tracks to Calculate Tau: 20, Min allowable R Squared: 0.1, Min Required Density Ratio: 2, Maximum Allowable Variability: 10 and Neighbour Mode: Free. For every recording, a background track count was calculated by averaging the track count of the 40 (10% of the total number of squares) least dense squares. Only squares for which the track count exceeded the Min Required Density Ratio of 2 were considered. For each square, the variability was calculated and only squares for which the variability was less than the Maximum Allowable Variability of 10 were considered. For squares meeting both the Minimum Required Density Ratio and Maximum Allowable Variability criteria, and containing at least the Minimum Tracks to Calculate Tau, kinetic parameters including k_{on}, k_{off}^{-1} and MSD were calculated as in Riera *et al*.[1],

or copied from the TrackMate Tracks table output (see 2.1 for detailed description of kinetic and statistical parameter outputs). Summary files were created using the ‘Compile Project‘ utility, creating an ‘All Recordings.csv‘ file, an ‘All Squares.csv‘ file, and an ‘All Tracks.csv‘ file. Statistical analysis and plotting using these merged files was performed using the `ggplot2` package in R.[24,25]

2.5 Supplementary Figures

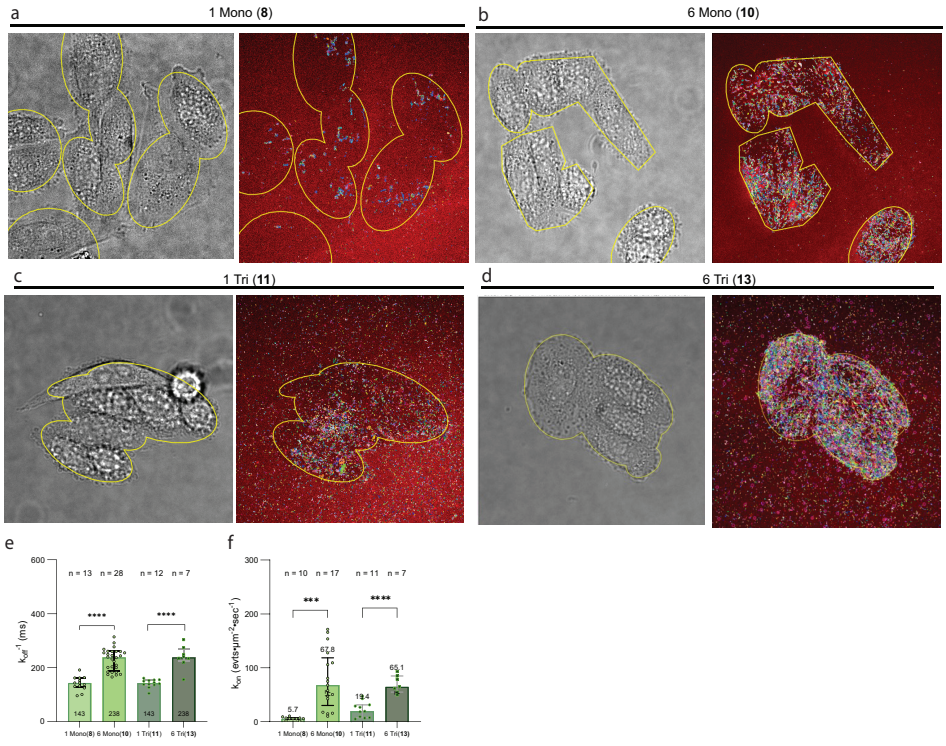

Figure S2.1: Manual analysis of glycan binding to CHO-MR using original Glyco-PAINT method (**a**) CHO-MR cells were incubated with 5 nM of fluorescent mannoside **8** in a live cell imaging chamber and a brightfield image was captured followed by a 2000 frame Glyco-PAINT recording. Closely-linked spots in subsequent frames were reconstructed into tracks representing binding events using the ImageJ TrackMate plugin and background filtering was performed by manual cell definition using ROI drawing (yellow outlines). (**b-d**) Identical analysis for glycans **10**, **11** and **13**, respectively. (**e**) The average k_{off}^{-1} for these events determined by fitting a one-phase exponential decay function over the binding event duration distribution histograms. (**f**) Quantification of the number of events per area which is a relative measure of k_{on}. n, depicts the number of recordings that were analyzed in total and were acquired over at least 3 biological replicates. However, not all recordings passed quality selection as detailed in methods section. Significance was assessed using two-way ANOVA followed by a Tukey post-hoc test. Tracks are colored randomly. Bar graphs and error bars represent mean ± interquartile range.

2.5. Supplementary Figures

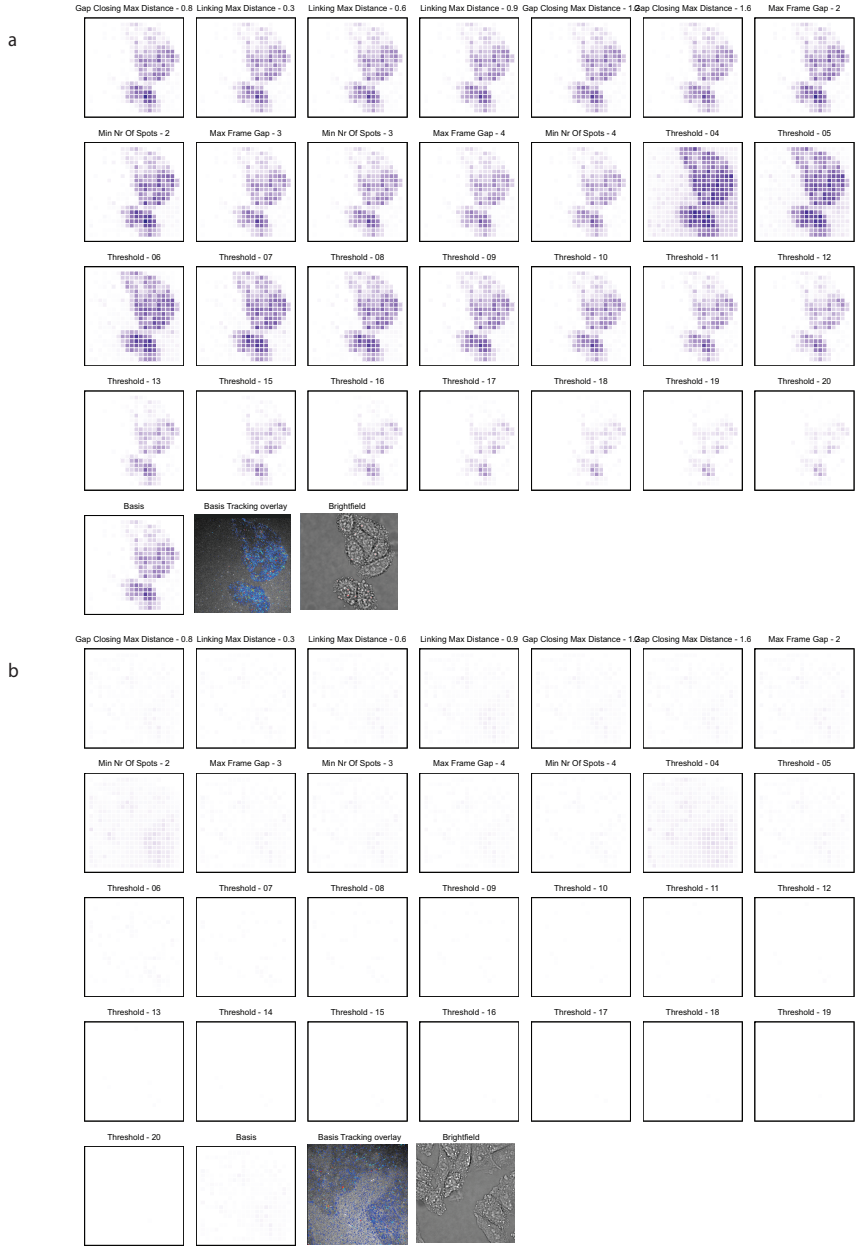

Figure S2.2

Figure S2.2: Tracking and spot detection parameter sweep for TrackMate analysis of Glyco-PAINT recordings. A single recording of glycan **13** binding to CHO-MR (**a**) or CHO-WT (**b**). Heatmap images of detected tracks (relative on-rate) per parameter setting are depicted. Recordings were analyzed using the indicated deviating parameter from the basis scenario, a 20×20 grid, and filtered with Density_Ratio > 2, R_Squared ≥ 0.9, and Nr_Tracks/Square > 20. Quantification of binding events can be found in **Figure 2.5**

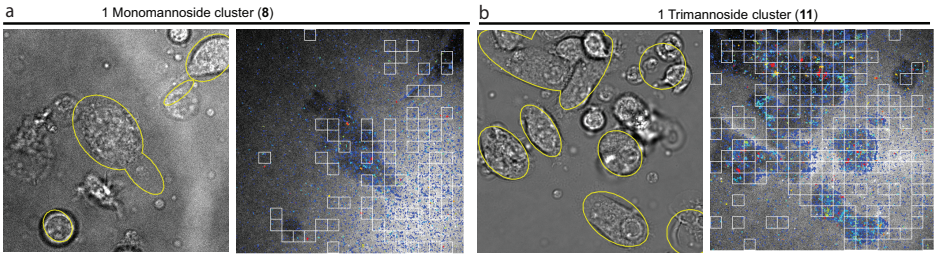

Figure S2.3: Glyco-PAINT-APP analysis of glycan binding to dendritic cells (a-b) Additional to main **Figure 2.7**. Brightfield and square-based detection of binding events for representative recordings of glycans **8** and **11**. Analysis and selection parameters are identical as in **Figure 2.7**.

Table 2.1: Glyco-PAINT-APP parameters. Standard pixel size $S = 0.160$ µm; image width $W = 512$ px; frame interval $\Delta t_f = 0.05$ s; total frames $F = 2000$.

Parameter	Formula	Derivation / Notes	Output Level	Units
Tau (τ, $k_{off}{}^{-1}$)	$N(t) = N_0 \cdot e^{-t/\tau}$	Track durations compiled into a histogram; one-phase exponential decay fit gives τ. Only when minimum track count is met.	Square / Recording	seconds
R^2 **(R_squared)**	$R^2 = 1 - \frac{SS_{\text{res}}}{SS_{\text{tot}}}$	Calculated with Tau. Near 1 = excellent fit; <0.5 = poor. User sets minimum.	Square / Recording	dimensionless (0–1)
Density (rel. k_{on})	$D_{\text{sq}} = \frac{N_{\text{tracks}}}{A \cdot t_{\text{rec}} \cdot C},\ A = \left(\frac{S \cdot W}{N_{\text{sq}}}\right)^2,\ t_{\text{rec}} = F \cdot \Delta t_f$	Normalized by square area A, total recording duration t_{rec}, and probe concentration C.	Square	tracks/µm^2/s/µM
Background Density	$D_{\text{bg}} = \overline{D_{\text{sq}}}\big\vert_{\text{lowest 10\%, } N>0}$	Lowest 10% of squares (by track count, > 0) for background reference of non-specific signal.	Recording	tracks/µm^2/s/µM
Density Ratio	$R_D = \frac{N_{\text{tracks, sq}}}{N_{\text{tracks, bg}}}$	Track count per square divided by background count. Above threshold implies biological relevance.	Square	dimensionless
Variability	$V = \frac{\sigma(n_{\text{sub}})}{\mu(n_{\text{sub}})}$	Coefficient of variation of track counts across sub-grid elements. Reflects spatial heterogeneity within a square.	Square	dimensionless
Diffusion Coeff. (D)	$\text{MSD} = \frac{1}{n}\sum_{i=1}^{n}[(x_i - x_0)^2 + (y_i - y_0)^2];$ $D = \frac{\text{MSD}}{2\, n_{\text{dim}}\, t}$	MSD per track vs. origin (x_0, y_0). n_{dim}=2, t=Δt_f. Median & mean per square.	Track → Square	µm^2/s
Diffusion Coeff. Ext (D_{ext})	$\text{MSD} = \frac{1}{n}\sum_{i=1}^{n}[(x_i - x_{i-1})^2 + (y_i - y_{i-1})^2];$ $D_{\text{ext}} = \frac{\text{MSD}}{2\, n_{\text{dim}}\, t}$	Consecutive-spot displacement variant, t=Δt_f. Median & mean per square.	Track → Square	µm^2/s
Track Duration	$\Delta t = (N_{\text{spots}} - 1) \times \Delta t_f$	Spot count × frame interval Δt_f. Per-square stats: median, max, total.	Track → Square	seconds
Long & Short Track Duration	$\Delta t_{\text{long}} = \text{median}(\Delta t \mid \text{top } 10\%);$ $\Delta t_{\text{short}} = \text{median}(\Delta t \mid \text{bottom } 10\%)$	Tracks ranked by Δt; median of longest/shortest 10% captures distribution tails.	Track → Square	seconds
Displacement	$d = \sqrt{(x_{\text{end}} - x_{\text{start}})^2 + (y_{\text{end}} - y_{\text{start}})^2}$	Euclidean start-to-end distance. Stats: median, max, total.	Track → Square	µm
Speed (Max & Mean)	$v_{\text{step}} = d(i, i-1)/\Delta t_f;\ v_{\text{max}} = \max(v_{\text{step}});$ $\bar{v} = \text{mean}(v_{\text{step}})$	Step-wise speed between consecutive spots. Stats: median/max of v_{max}; median/max of $\bar{v}$ across tracks.	Track → Square	µm/s
Confinement Ratio	$CR = d_{\text{net}}/L_{\text{total}}$	Net displacement over total path length. Near 1 = directed; near 0 = confined/random.	Track → Square	dimensionless (0–1)

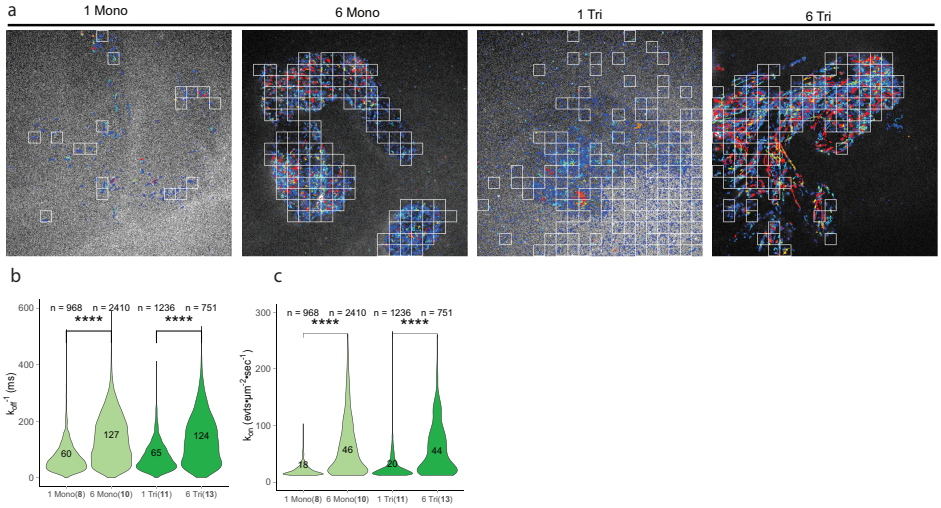

Figure S2.4: Glyco-PAINT-APP analysis of glycan binding to CHO-MR (**a**) Square-based detecion of **8**, **10**, **11** and **13** binding to CHO-MR for identical recordings as in shown in **Figure 2.3a** using ROI analysis (**b**) Square-based detection of **8**, **10**, **11** and **13** binding to CHO-MR for identical recordings as in shown in **Figure S2.1** using ROI analysis. **b** The number of events per area which is a relative measure of k_{on}. n, depicts the number of squares that were analyzed per violin. Significance was assessed using two-way ANOVA followed by a Tukey post-hoc test.

References

(1) Riera, R.; Hogervorst, T. P.; Doelman, W.; Ni, Y.; Pujals, S.; Bolli, E.; Codée, J. D. C.; van Kasteren, S. I.; Albertazzi, L. Single-molecule imaging of glycan–lectin interactions on cells with Glyco-PAINT. *Nature Chemical Biology* **2021**, *17*, 1281–1288.

(2) Schnitzbauer, J.; Strauss, M. T.; Schlichthaerle, T.; Schueder, F.; Jungmann, R. Super-resolution microscopy with DNA-PAINT. *Nature Protocols* **2017**, *12*, 1198–1228.

(3) Tachado, S. D.; Zhang, J.; Zhu, J.; Patel, N.; Cushion, M.; Koziel, H. Pneumocystis-mediated IL-8 release by macrophages requires coexpression of mannose receptors and TLR2. *Journal of Leukocyte Biology* **2007**, *81*, 205–211.

(4) Li, F.; Wang, H.; Li, Y.-Q.; Gu, Y.; Jia, X.-M. C-type lectin receptor 2d forms homodimers and heterodimers with TLR2 to negatively regulate IRF5-mediated antifungal immunity. *Nature Communications* **2023**, *14*, 6718.

(5) Geijtenbeek, T. B. H.; Gringhuis, S. I. Signalling through C-type lectin receptors: shaping immune responses. *Nature Reviews Immunology* **2009**, *9*, 465–479.

(6) Den Dunnen, J.; Gringhuis, S. I.; Geijtenbeek, T. B. H. Innate signaling by the C-type lectin DC-SIGN dictates immune responses. *Cancer immunology, immunotherapy: CII* **2009**, *58*, 1149–1157.

REFERENCES

(7) Park, D. D.; Chen, J.; Kudelka, M. R.; Jia, N.; Haller, C. A.; Kosaraju, R.; Premji, A. M.; Galizzi, M.; Nairn, A. V.; Moremen, K. W.; Cummings, R. D.; Chaikof, E. L. Resident and elicited murine macrophages differ in expression of their glycomes and glycan-binding proteins. *Cell Chemical Biology* **2021**, *28*, 567–582.e4.

(8) Tommasone, S.; Allabush, F.; Tagger, Y. K.; Norman, J.; Köpf, M.; Tucker, J. H. R.; Mendes, P. M. The challenges of glycan recognition with natural and artificial receptors. *Chemical Society Reviews* **2019**, *48*, 5488–5505.

(9) Inaba, K.; Inaba, M.; Romani, N.; Aya, H.; Deguchi, M.; Ikehara, S.; Muramatsu, S.; Steinman, R. M. Generation of large numbers of dendritic cells from mouse bone marrow cultures supplemented with granulocyte/macrophage colony-stimulating factor. *The Journal of Experimental Medicine* **1992**, *176*, 1693–1702.

(10) Van den Dries, K.; van Helden, S. F. G.; Riet, J. t.; Diez-Ahedo, R.; Manzo, C.; Oud, M. M.; van Leeuwen, F. N.; Brock, R.; Garcia-Parajo, M. F.; Cambi, A.; Figdor, C. G. Geometry sensing by dendritic cells dictates spatial organization and PGE2-induced dissolution of podosomes. *Cellular and Molecular Life Sciences: CMLS* **2011**, *69*, 1889–1901.

(11) Gawden-Bone, C.; West, M. A.; Morrison, V. L.; Edgar, A. J.; McMillan, S. J.; Dill, B. D.; Trost, M.; Prescott, A.; Fagerholm, S. C.; Watts, C. A crucial role for β2 integrins in podosome formation, dynamics and Toll-like-receptor-signaled disassembly in dendritic cells. *Journal of Cell Science* **2014**, *127*, 4213–4224.

(12) Ershov, D.; Phan, M.-S.; Pylvänäinen, J. W.; Rigaud, S. U.; Le Blanc, L.; Charles-Orszag, A.; Conway, J. R. W.; Laine, R. F.; Roy, N. H.; Bonazzi, D.; Duménil, G.; Jacquemet, G.; Tinevez, J.-Y. TrackMate 7: integrating state-of-the-art segmentation algorithms into tracking pipelines. *Nature Methods* **2022**, *19*, 829–832.

(13) Rillahan, C. D.; Paulson, J. C. Glycan Microarrays for Decoding the Glycome. *Annual Review of Biochemistry* **2011**, *80*, 797–823.

(14) Shinohara, Y.; Furukawa, J.-i. Surface plasmon resonance as a tool to characterize lectin-carbohydrate interactions. *Methods in Molecular Biology (Clifton, N.J.)* **2014**, *1200*, 185–205.

(15) Kéry, V.; Krepinský, J. J.; Warren, C. D.; Capek, P.; Stahl, P. D. Ligand recognition by purified human mannose receptor. *Archives of Biochemistry and Biophysics* **1992**, *298*, 49–55.

(16) E. Tholen, M. M.; P. Tas, R.; Wang, Y.; Albertazzi, L. Beyond DNA: new probes for PAINT super-resolution microscopy. *Chemical Communications* **2023**, *59*, 8332–8342.

(17) Tas, R. P.; Albertazzi, L.; Voets, I. K. Small Peptide–Protein Interaction Pair for Genetically Encoded, Fixation Compatible Peptide-PAINT. *Nano Letters* **2021**, *21*, 9509–9516.

(18) Albertazzi, L.; Heilemann, M. When Weak Is Strong: A Plea for Low-Affinity Binders for Optical Microscopy. *Angewandte Chemie International Edition* **2023**, *62*, e202303390.

(19) Dustin, M. L. Recent advances in understanding TCR signaling: a synaptic perspective. *Faculty Reviews* **2023**, *12*.

(20) Lin, J. J. Y.; Low-Nam, S. T.; Alfieri, K. N.; McAffee, D. B.; Fay, N. C.; Groves, J. T. Mapping the stochastic sequence of individual ligand-receptor binding events to cellular activation: T cells act on the rare events. *Science Signaling* **2019**, *12*, eaat8715.

(21) Yu, X.; Orr, C. M.; Chan, H. T. C.; James, S.; Penfold, C. A.; Kim, J.; Inzhelevskaya, T.; Mockridge, C. I.; Cox, K. L.; Essex, J. W.; Tews, I.; Glennie, M. J.; Cragg, M. S. Reducing affinity as a strategy to boost immunomodulatory antibody agonism. *Nature* **2023**, *614*, 539–547.

(22) Baycin-Hizal, D. et al. Proteomic Analysis of Chinese Hamster Ovary Cells. *Journal of Proteome Research* **2012**, *11*, 5265–5276.

(23) Martinez-Pomares, L.; Reid, D. M.; Brown, G. D.; Taylor, P. R.; Stillion, R. J.; Linehan, S. A.; Zamze, S.; Gordon, S.; Wong, S. Y. Analysis of mannose receptor regulation by IL-4, IL-10, and proteolytic processing using novel monoclonal antibodies. *Journal of Leucocyte Biology* **2003**, *73*, 604–613.

(24) R Core Team, *R: A Language and Environment for Statistical Computing*; R Foundation for Statistical Computing: Vienna, Austria, 2023.

(25) Wickham, H., *ggplot2: Elegant Graphics for Data Analysis*; Springer-Verlag New York: 2016.